

Shape and surface structure of gold nanoparticles under oxidizing conditions

Hongqing Shi and Catherine Stampfl

School of Physics, The University of Sydney, Sydney, New South Wales 2006, Australia

(Received 14 January 2008; published 24 March 2008)

We perform density-functional theory calculations to investigate the adsorption of oxygen at the Au(100) and Au(110) surfaces. For the clean surfaces, we find that the added-row $(5 \times 1)/\text{Au}(100)$ structure is more stable than the unreconstructed $(1 \times 1)/\text{Au}(100)$ surface and the missing-row $(2 \times 1)/\text{Au}(110)$ structure is more stable than the unreconstructed $(1 \times 1)/\text{Au}(110)$ surface, which is consistent with experimental results. For oxygen adsorption on Au(100), the most stable structure is predicted to be a low coverage (~ 0.1 ML) on the added-row reconstructed surface, while for adsorption on Au(110), the most stable configuration of those considered is a (2×1) missing-row structure with 1 ML coverage of oxygen. From these results, together with those of our previous investigations into the O/Au(111) system, we use the Wulff construction to predict the nanoparticle shape as a function of oxygen chemical potential, which we correlate with pressure (p) and temperature (T). For low values of the oxygen chemical potential (< -0.6 eV, corresponding, e.g., to $p = 1$ atm and $T > 600$ K), the nanoparticle consists of clean (111) facets. For slightly higher values, clean (111) facets still dominate but there are small regions of (110) facets, which are covered with the (2×1) -2O reconstruction. With progressively increasing values of the chemical potential (e.g., from -0.4 to -0.18 eV, corresponding to, e.g., $p = 1$ atm and $T = 420$ – 200 K), the (111) facets become covered with a thin oxide-like structure, and the (110) regions with the (2×1) -2O/(110) surface reconstruction become larger and finally dominate. These findings indicate that for low temperature oxidation reactions, where gold nanoparticles have been reported to be surprisingly active, such thin “surface-oxide-like” structures on the (111) and (110) surfaces could possibly play a role in the behavior of the nanogold catalysts.

DOI: [10.1103/PhysRevB.77.094127](https://doi.org/10.1103/PhysRevB.77.094127)

PACS number(s): 68.47.Gh, 68.43.Bc, 82.65.+r, 82.60.Qr

I. INTRODUCTION

In contrast to the long held view that gold is catalytically inert, it is now well known that Au nanoparticles both supported on reducible oxide supports and unsupported are notably more active than other transition metals for low temperature oxidation of CO and other heterogeneous catalytic reactions.^{1–4} This has stimulated huge efforts in an attempt to understand the mechanisms responsible for the high activity, including investigations into the nature of oxygen on gold surfaces.⁴ The active site, however, for nanoparticle gold catalysts remains under debate.⁵ Clearly, the catalytically relevant sites will depend crucially on the exposed surface orientations of the crystallite.^{6,7}

Considerable investigations have been carried out, both experimentally and theoretically, into the interaction of oxygen with the Au(111) surface.^{8,10–32} Recently, we predicted, based on density-functional theory (DFT) calculations for the adsorption of oxygen at Au(111),⁸ that a thin surface-oxide-like configuration is the most favorable structure of those considered. Furthermore, this structure was predicted to be stable up to temperatures of around 420 K at atmospheric pressure. Although the clean (111) surface (which is reconstructed into a “herringbone” structure⁹) has the lowest surface energy of the low-index surfaces, the adsorption of adparticles, such as oxygen, can change the relative stability and so it is important to consider the surfaces energies of other low-index orientations. The Au(100) clean surface has been experimentally studied using low energy electron diffraction (LEED),³³ He-ion scattering,³⁴ and scanning tunneling microscopy (STM).³⁵ All the experimental results indicate a reconstructed, slightly rotated, and densely packed

triangular structure for the topmost layer. Originally, a (1×5) reconstruction was suggested, which seemed to agree well with high-resolution STM images, but other models with larger surface unit cells have also been put forward.⁴ From embedded-atom calculations, Daw and Baskes predicted that a (1×1) reconstruction was favorable, which has a slightly buckled quasitriangular surface with 20% higher surface atomic density than the unreconstructed (1×1) surface, which agrees semiquantitatively with the experimental results.³⁶ *Ab initio* studies performed by Fiorentini *et al.*³⁷ show that a close-packed quasihexagonal reconstruction is possible for the (100) surface of the late $5d$ metals, Ir, Pt, and Au. For the clean Au(110) surface, both glancing-incidence x-ray diffraction³⁸ and high-resolution electron microscopy³⁹ confirmed the “missing-row” model of reconstructed Au(110). A later LEED intensity analysis of the reconstructed $(1 \times 2)/\text{Au}(110)$ surface reported a modification of the missing-row model, namely, that it contained considerable distortions, which are at least three layers deep.⁴⁰

With regard to O adsorption on Au(100) and Au(110), Davis and Goodman observed that oxygen desorbs recombinatively in a single peak at 470 K from Au(100),²¹ and no ordered overlayer structure was observed. By using an electron bombardment of physisorbed and condensed oxygen molecules on Au(110)- (1×2) at 28 K, chemisorbed atomic oxygen was produced.⁴¹ This structure was investigated with UV photoelectron spectroscopy (UPS), where it was found that the electronic structure of chemisorbed oxygen bears a strong resemblance to that of gold oxide (Au_2O_3). Coverages beyond one monolayer were associated with gold oxide. It was found that chemisorbed oxygen reacts vigorously with carbon monoxide even below 100 K.⁴¹

In the present paper, we examine the interaction of atomic oxygen and the stability of oxygen adsorption and thin surface oxides on Au(100) and Au(110) for a range of coverages and atomic geometries. By using these results, together with those of our earlier study of the O/Au(111) system, we predict the nanomorphology of Au particles in an oxygen atmosphere by using the Wulff construction. Among other things, the calculations indicate that under the conditions of technically low temperature oxidation reactions, e.g., $p=1$ atm and $200\text{ K} < T < 420\text{ K}$, the nanoparticles are dominated by (110) and (111) facets, which are covered with a very thick surface-oxide-like structure. The paper is organized as follows: In Sec. II, we give details of the first-principles DFT total-energy calculations, including a brief description of the *ab initio* atomistic thermodynamics approach. In Sec. III, results are presented for the clean Au(100) and Au(110) surfaces. The results for O/Au(100) systems, including atomic and electronic structures and adsorption energies, are presented in Sec. IV, while those for O/Au(110) are presented in Sec. V. The discussion, including the results of the surface free energy and associated temperature and pressure dependence, and the predicted nanoparticle shapes, is given in Sec. VI. The conclusion is given in Sec. VII and convergence tests are described in the Appendix.

II. CALCULATION METHOD AND DEFINITIONS

The calculations are performed using the DFT total-energy Vienna *ab initio* simulation package (VASP).^{42–44} We employ the projector augmented-wave method^{45,46} (PAW) and the generalized-gradient approximation (GGA) for the exchange-correlation functional.⁴⁷ The wave functions are expanded in a plane-wave basis set with an energy cutoff of 36.75 Ry (500 eV). The Fermi level and/or electronic occupancies are smeared by a Gaussian function with a temperature broadening of $k_B T^{\text{el}} = 0.1$ eV (k_B is the Boltzmann constant) and the total energy is extrapolated to zero temperature. The PAW potential is generated taking scalar relativistic corrections into account. We use symmetric slabs for the clean surface energy calculations, where the Au(100) surface is described by a six-layer slab and the unreconstructed Au(110) surface by a nine-layer slab. For Au(100), we relax the two topmost and bottom two atomic layers, and keep the center two layers fixed at the bulk positions. For Au(110), we relax the three topmost and bottom three atomic layers, and keep the center three layers fixed at the bulk positions. For the (2×1) missing-row reconstruction of the Au(110) surface, we use 11 atomic layers, keeping the center three layers fixed at the bulk positions and relaxing all other atoms. The (1×1) /Au(111) surface is modeled by a seven-layer slab, with the top and bottom two layers relaxed. All slabs are separated by more than 15 Å of vacuum space. For the adsorption studies, oxygen is placed on one side of the slab, where the induced dipole moment is taken into account by applying a dipole correction.⁴⁸ We allow atomic relaxation of all gold atoms in the top four layers of the (100) surface and the top five layers of the (110) surface, plus the oxygen atoms. The final forces on the atoms are less than 0.01 eV/Å. For the \mathbf{k} -point sampling, $4 \times 20 \times 1$ and 4

$\times 12 \times 1$ meshes are used for the (5×1) /Au(100) and (2×1) /Au(110) surface unit cells (SUCs), which generate 33 and 21 \mathbf{k} points in the surface irreducible Brillouin zone (IBZ) for the Brillouin zone integration, respectively. Equivalent \mathbf{k} points are used for all of the surface structures studied to maximize the accuracy. Convergence tests were performed regarding the energy cutoff, \mathbf{k} -point sampling, the number of layers, as well as cell size, and are reported in the Appendix. The results, together with those tests reported in Ref. 8 for O/Au(111), demonstrate the high accuracy of our calculations.

We evaluate the surface energy as

$$\sigma_{\text{surf}} = \frac{1}{2A} (E_{\text{surf}}^{\text{tot}} - nE_{\text{bulk}}^{\text{tot}}), \quad (1)$$

where $E_{\text{surf}}^{\text{tot}}$ and $E_{\text{bulk}}^{\text{tot}}$ are the total energies of the (fully relaxed) surface system and a gold atom in bulk, respectively. n is the number of Au atoms in the corresponding slab and A is the corresponding surface area of the employed SUC.

The average adsorption energy per oxygen atom is defined as

$$E_{\text{ad}} = -\frac{1}{N_{\text{O}}} [E_{\text{O/Au}} - (E_{\text{Au}} + N_{\text{O}}E_{\text{O}}) + \Delta N_{\text{Au}}E_{\text{Au}}^{\text{bulk}}], \quad (2)$$

where N_{O} is the number of oxygen atoms in the SUC, and $E_{\text{O/Au}}$, E_{Au} , and E_{O} represent the total energy of the adsorbate-substrate system, the clean unreconstructed surface, and the free oxygen atom, respectively. For oxygen adsorption on an unreconstructed surface, ΔN_{Au} is equal to zero. For surface structures involving a different number of Au atoms compared to the clean unreconstructed reference slab, ΔN_{Au} is the number of Au atoms missing from, or added to, the corresponding reference surface. $E_{\text{Au}}^{\text{bulk}}$ is the total energy of a gold atom in bulk. This term appears since the missing (or added) Au atoms are assumed to be rebound at (dissociated from) kink sites at steps, which contribute an energy equal to that of a bulk Au atom.^{49,50} The adsorption energy E_{ad} is defined such that a positive number indicates that the adsorption is exothermic (stable or metastable) and a negative number indicates endothermic (unstable).

We consider the surface in contact with an oxygen atmosphere, which is described by an oxygen pressure p and a temperature T , and calculate the Gibbs surface free energy of adsorption as

$$\gamma(T, p) = (G_{\text{O/Au}}^{\text{slab}} - G_{\text{Au}}^{\text{slab}} + \Delta N_{\text{Au}}\mu_{\text{Au}} - N_{\text{O}}\mu_{\text{O}})/A. \quad (3)$$

$G_{\text{O/Au}}^{\text{slab}}$ and $G_{\text{Au}}^{\text{slab}}$ are the Gibbs free energies of the O/Au surface under consideration and that of the clean unreconstructed substrate reference system, respectively. μ_{Au} and μ_{O} are the chemical potentials of a Au and an O atom, respectively, and A is the surface area. We take $\mu_{\text{Au}} = g_{\text{Au-bulk}}$, the free energy of a bulk Au atom. For pressures not exceeding about 100 atm, the contribution from the pV term in Gibbs free energy is negligible. In this work, we neglect vibrational contributions. In our previous study for O/Au(111), we found that for the lowest energy surface structure, vibrational contributions for $T < 600\text{ K}$ were not greater than ± 3 meV.

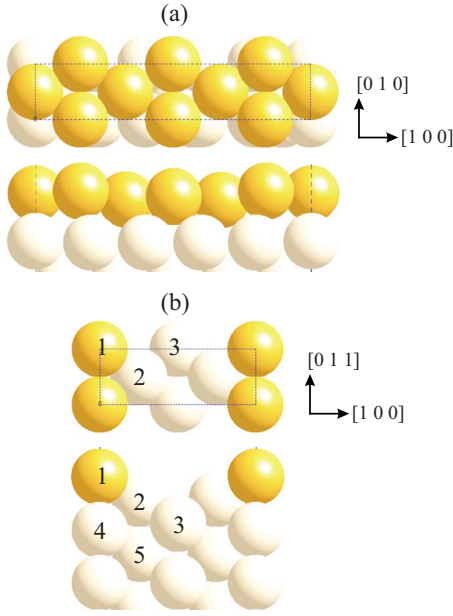


FIG. 1. (Color online) Top (upper) and side (lower) views of the atomic geometry of (a) the added-atom $(5 \times 1)/\text{Au}(100)$ structure and (b) the missing-row $(2 \times 1)/\text{Au}(110)$ surface. Darker (yellow) and light (pale yellow) spheres indicate Au atoms in the topmost and lower lying layers, respectively. The SUCs are indicated. (The numbers on the atoms are labels referred to in Table II.)

Thus, the total energies are the predominant term in the Gibbs free energies.

The T and p dependence is mainly given by μ_{O} , i.e., by the O_2 gas phase atmosphere, as follows:⁵¹

$$\mu_{\text{O}}(T, p) = \frac{1}{2} \left[E_{\text{O}_2}^{\text{total}} + \tilde{\mu}_{\text{O}_2}(T, p^0) + k_B T \ln \left(\frac{p_{\text{O}_2}}{p^0} \right) \right], \quad (4)$$

where p^0 corresponds to atmospheric pressure and $\tilde{\mu}_{\text{O}_2}(T, p^0)$ includes the contribution from rotations and vibrations of the molecule, as well as the ideal-gas entropy at 1 atm.⁵¹ $E_{\text{O}_2}^{\text{total}}$ is the total energy of the oxygen molecule. We also consider the Gibbs free surface energy,

$$\sigma_{\text{surf}}^{\text{O/Au}}(T, p) = (E_{\text{O/Au}} - N_{\text{Au}}\mu_{\text{Au}} - N_{\text{O}}\mu_{\text{O}})/A - \sigma_{\text{surf}}^{\text{unrel.clean}}. \quad (5)$$

Here, N_{Au} is the number of Au atoms in the O/Au system. The surface energy of the clean unrelaxed (and unrecon-

structed) surface, $\sigma_{\text{surf}}^{\text{unrel.clean}}$, is subtracted because an asymmetric surface slab is used in the adsorption calculations. It can be shown that Eq. (5) is equivalent to $\sigma_{\text{surf}}^{\text{O/Au}}(T, p) = \gamma(T, p) + \sigma_{\text{surf}}$.

III. Au(100) AND Au(110) CLEAN SURFACES

The calculated lattice constant of face-centered-cubic gold is 4.175 Å and the bulk modulus is 132 GPa. The corresponding experimental values are 4.08 Å and 170 GPa.⁵² Thus, the DFT-GGA result slightly overestimates the former and, correspondingly, underestimates the latter. The calculated value agrees very well with previous DFT-GGA results, where values of 4.19 Å and 132 GPa were reported.⁵³ The theoretical (DFT-GGA) cohesive energy of Au is 3.05 eV/atom and the value reported from VASP by using the local density approximation (LDA) is 4.39 eV/atom.⁵⁴ The experimental result is 3.81 eV/atom.⁵² The GGA thus underestimates and the LDA overestimates the cohesive energy. In our GGA calculations for the cohesive energy, the free gold atom has been calculated including spin polarization.

We calculate the surface energies for the relaxed unreconstructed (1×1) surfaces of Au(100), Au(110), and Au(111), as well as that for the added-atom $(5 \times 1)/\text{Au}(100)$ surface^{36,37} [see Fig. 1(a)] and the missing-row $(2 \times 1)/\text{Au}(110)$ surface⁴⁰ [see Fig. 1(b)]. [Note that for the latter two surface unit cells, the convention is opposite to some used in the literature; i.e., (1×5) and (1×2) have been used to denote these structures in some publications, but they are identical to the ones discussed here.] The surface energies are given in Table I. It can be seen that the added-atom $(5 \times 1)/\text{Au}(100)$ and missing-row $(2 \times 1)/\text{Au}(110)$ surfaces are more stable than the corresponding unreconstructed (1×1) clean surface (by 0.005 eV/Å²), which is consistent with experimental results, which find the clean surfaces to be reconstructed.^{33–35,38–40} For the $(2 \times 1)/\text{Au}(110)$ missing-row surface, the interlayer distance between the top two layers is contracted significantly by 21%. The two atoms in the third layer [see Fig. 1(b), atoms 3 and 4] exhibit a rumbling of 0.33 Å perpendicular to the surface, which is in agreement with the experimental value of 0.24 Å.⁴⁰ The bond lengths between the metal atoms and their deviation relative to the bulk values are listed in Table II. Our calculated results agree very well with the results from a LEED intensity analysis.⁴⁰ The bond length does not vary as much as the large contraction of the interlayer distance between the top two layers due

TABLE I. Surface energy, σ_{surf} (in eV/Å²), for the relaxed unreconstructed and reconstructed clean surfaces, the first (d_{12}) and second (d_{23}) interlayer distances (in Å), and the deviation (Δ) from the corresponding bulk values (in %).

Clean surface	d_{12}	Δd_{12}	d_{23}	Δd_{23}	σ_{surf}
$(1 \times 1)/\text{Au}(110)$	1.28	-13.3	1.60	8.40	0.057
$(2 \times 1)/\text{Au}(110)$ missing-row	1.16	-21.4	1.50	1.63	0.052
$(1 \times 1)/\text{Au}(100)$	2.01	-3.7	2.07	-0.84	0.054
$(5 \times 1)/\text{Au}(100)$ added-atom	2.51	20.2	2.07	-0.84	0.049
$(1 \times 1)/\text{Au}(111)$	2.44	1.2	2.40	-0.41	0.045

TABLE II. Calculated Au-Au bond lengths (in Å), deviation from the bulk value Δd (in %), and corresponding experimental values for the $(2 \times 1)/\text{Au}(110)$ missing-row surface structure. Atoms are labeled as in Fig. 1(b).

	This work		Expt. ^a	
	Bond length	Δd	Bond length	Δd
Au1-Au2	2.84	-3.7	2.80	-2.8
Au1-Au4	2.82	-4.4	2.74	-5.0
Au2-Au3	2.85	-3.4	2.79	-3.3
Au2-Au4	3.08	4.3	3.01	4.4
Au2-Au5	2.99	1.2	2.94	2.0
Au3-Au5	2.99	1.4	2.96	2.7
Au4-Au5	2.93	-0.6	2.84	-1.5

^aReference 40.

to compensation from the lateral deviations in the second layer and the buckling in the third layer.

IV. OXYGEN ADSORPTION ON Au(100)

For oxygen adsorption on the Au(100) surface, we considered various structures (see Fig. 2). We also investigated an oxygen structure involving on-surface and subsurface adsorption (not shown in Fig. 2), reported as “the most stable (2×2) structure” considered for O on Ag(100) [see Fig. 5(b) of Ref. 55] and a “ $(2\sqrt{2} \times \sqrt{2})$ missing-row reconstruction,” which was studied for O on Ag(100) (see Fig. 3 of Ref. 56). In the former structure, one O atom is in the hollow site and another O atom is in a “subhollow” site, while two additional O atoms are located in subsurface octahedral sites. The $(2\sqrt{2} \times \sqrt{2})$ missing-row reconstruction consists of two oxygen atoms in the pseudo-three-fold hollow sites and two subsurface O atoms in the subsurface octahedral site.⁵⁶ However, for Au(100), we find that both these structures are less

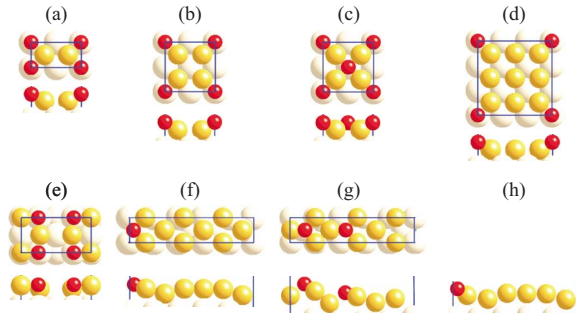


FIG. 2. (Color online) Top (upper) and side (lower) views of the atomic geometries considered for O/Au(100). (a) (2×1) -O, (b) (2×2) -O, (c) (2×2) -2O or $c(2 \times 2)$ -O, (d) (3×3) -O for oxygen in the hollow site, (e) missing-row $(2\sqrt{2} \times \sqrt{2})R45^\circ$ -O, (f) added-atom (5×1) -O, (g) added-atom (5×1) -2O, and (h) added-atom (5×2) -O. The small dark (red), large gray (yellow), and light gray (pale yellow) spheres correspond to oxygen atoms, uppermost Au atoms, and second layer Au atoms, respectively. The SUCs are indicated.

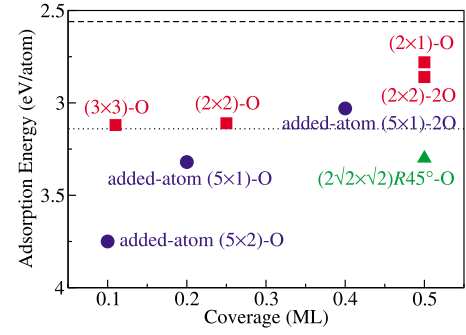


FIG. 3. (Color online) Calculated average adsorption energy of oxygen on Au(100) versus coverage, with respect to atomic oxygen. The upper and lower horizontal lines represent the experimental (2.56 eV) and theoretical (3.14 eV) values of the O_2 binding energy per atom, respectively.

stable than the others we considered and they are not discussed further. It is interesting to note the significant rumpling of the top Au layer that oxygen adsorption induces for the added-atom (5×1) -O, (5×1) -2O, and (5×2) -O structures [see Figs. 2(f)–2(h)]. The average oxygen adsorption energies [cf. Eq. (2)], with respect to atomic oxygen, are plotted in Fig. 3 as a function of coverage and the values are given in Table III. It can be seen that the structure involving on-surface oxygen adsorption in the quasi-three-fold hollow site of the added-atom (5×2) surface [Fig. 2(h)] has the most favorable energy.

The bond lengths between the oxygen atom and its three neighboring gold atoms for the lowest energy structure are 2.11, 2.11, and 2.20 Å, respectively. We also consider the difference electron density, $n^\Delta(\mathbf{r})$,

$$n^\Delta(\mathbf{r}) = n(\mathbf{r}) - n^0(\mathbf{r}) - n^O(\mathbf{r}), \quad (6)$$

where $n(\mathbf{r})$ is the total electron density of the adsorbate-substrate system, and $n^0(\mathbf{r})$ and $n^O(\mathbf{r})$ are the electron densities of the clean substrate and the free oxygen atom, respectively, where the atomic geometry of the substrate is that of

TABLE III. Average adsorption energy (in eV), E_{ad} , per O atom for the O/Au(100) structures shown in Fig. 2. All energies are given with respect to the free oxygen atom (which includes spin polarization). Also given are the number of O atoms (N_{O}), the number of topmost Au atoms ($N_{\text{Au-top}}$) in the SUC, and the corresponding coverage (in ML).

Structure	N_{O}	$N_{\text{Au-top}}$	Coverage	E_{ad}
(2×1) -O	1	2	0.50	2.78
(2×2) -O	1	4	0.25	3.11
(2×2) -2O	2	4	0.50	2.86
(3×3) -O	1	9	0.11	3.12
Missing-row $(2\sqrt{2} \times \sqrt{2})R45^\circ$ -O	2	3	0.50	3.30
Added-atom (5×1) -O	1	6	0.20	3.32
Added-atom (5×1) -2O	2	6	0.40	3.03
Added-atom (5×2) -O	1	12	0.10	3.75

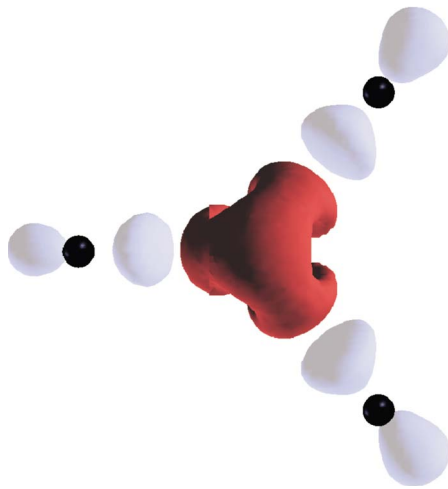


FIG. 4. (Color online) Difference electron density for the added-atom (5×2) -O/Au(100) structure. The dark (red) isosurfaces indicate an increase in electron density, and the light (pale blue) isosurfaces represent a depletion. The black spheres indicate the position of the gold atoms. The value of the isospheres is $\pm 2.0 \times 10^{-5} e/\text{\AA}^3$.

the relaxed adsorbate system (but without the O atoms). This quantity then shows from which regions the electron density has been depleted and increased due to O adsorption on the surface. The calculated difference electron density distribution for the (5×2) -O structure is shown in Fig. 4. Qualitatively, the features are very similar to those obtained for oxygen adsorption on Au(111) at low coverage, as reported in Ref. 8 (Fig. 3), with a depletion of the Au $5d$ states and an increase in the O $2p$ states, as well as a polarization of the O atoms. In Fig. 5, we show the corresponding projected density of states (PDOS). It can be seen that there is a hybridization between the O $2p$ and Au $5d$ orbitals. The valence PDOS for the O atom shows that there are two main regions of high electron density below the Fermi level. These correspond to bonding- and antibonding-like states. The bonding states are located near the bottom of (and within) the Au $5d$

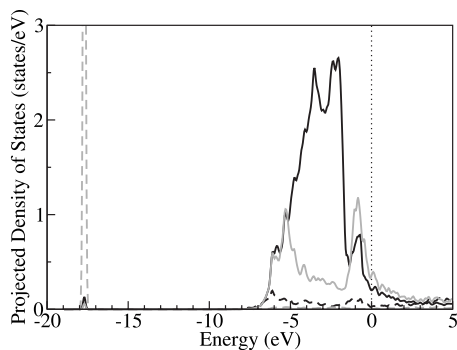


FIG. 5. PDOS for the added-atom (5×2) -O/Au(100) structure. The Au PDOS of the first metal layer atoms that are bonded to oxygen are indicated by dashed ($6s$) and solid ($5d$) dark lines, respectively. The PDOS of the O $2s$ and $2p$ states are represented by the dashed and solid gray lines, respectively. The Fermi energy is denoted by the vertical line.

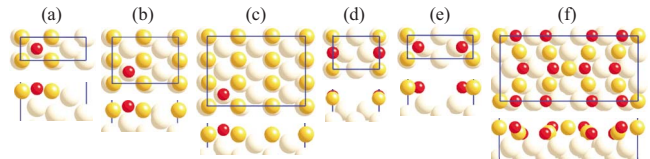


FIG. 6. (Color online) Top (upper) and side (lower) views of the atomic geometries considered for O/Au(110): (a) (2×1) -O, (b) (2×2) -O, (c) (3×3) -O, (d) missing-row (1×2) -O, (e) missing-row (2×1) -2O, and (f) a $c(2 \times 6)$ structure. Small dark (red), large gray (yellow), and light gray (pale yellow) spheres represent O atoms, Au atoms in the uppermost layer, and deeper lying Au atoms, respectively. The SUCs are indicated.

band, and the antibonding states near the top of it are largely occupied, thus preventing a strong covalent bonding. The PDOS is also qualitatively similar to that obtained for oxygen adsorption on Au(111) at low coverage, as reported in Ref. 8 (Fig. 4).

V. OXYGEN ADSORPTION ON Au(110)

For oxygen adsorption on the Au(110) surface, we considered six structures (see Fig. 6). Three of these configurations were stimulated by O structures that form on other noble metal (110) surfaces, in particular, the missing-row (1×2) -O structure [Fig. 6(d)] has been reported for Ag(110),⁵⁷ the missing-row (2×1) -2O structure [Fig. 6(e)] has been reported for Pt(110),⁵⁸ and the $c(2 \times 6)$ structure [Fig. 6(f)] has been reported for Cu(110).⁵⁹ The average adsorption energies, with respect to atomic oxygen, are plotted in Fig. 7 as a function of coverage and the values are given in Table IV. It can be seen that the missing-row (2×1) -2O structure [Fig. 6(e)] has the most favorable energy. It is interesting to note for this structure that the “surface-oxide” layer is composed of (edge-sharing) AuO_4 units that contain four oxygen atoms around one gold atom, while the O atoms are twofold coordinated to Au. This AuO_4 unit is rather similar to that constituting the atomic network of gold oxide Au_2O_3 .⁶⁰ The bond length between the oxygen atom and its nearest neigh-

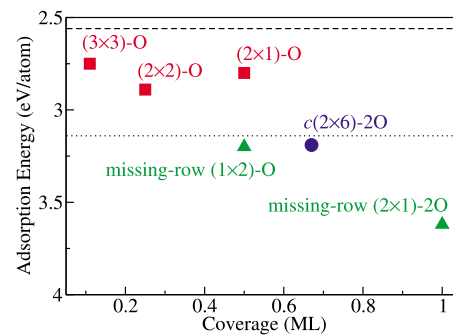


FIG. 7. (Color online) Calculated average adsorption energy of oxygen on Au(110) versus coverage, with respect to atomic oxygen. The upper and lower horizontal lines represent the experimental (2.56 eV) and theoretical (3.14 eV) values of the O_2 binding energy per atom.

TABLE IV. Average adsorption energy (in eV), E_{ad} , per O atom for the considered O/Au(110) structures shown in Fig. 6. All energies are given with respect to the free oxygen atom. Also given are the number of O atoms (N_{O}), the number of topmost Au atoms ($N_{\text{Au-top}}$) in the SUC, and the corresponding coverage (in ML).

Structure	N_{O}	$N_{\text{Au-top}}$	Coverage	E_{ad}
$(2 \times 1)\text{-O}$	1	2	0.50	2.80
$(2 \times 2)\text{-O}$	1	4	0.25	2.89
$(3 \times 3)\text{-O}$	1	9	0.11	2.75
Missing-row $(1 \times 2)\text{-O}$	1	1	0.50	3.20
Missing-row $(2 \times 1)\text{-2O}$	2	1	1.00	3.62
$c(2 \times 6)$	8	10	0.67	3.19

bor gold atom for the lowest energy missing-row $(2 \times 1)\text{-2O}$ structure is 2.03 Å, which is very close to the value of 2.01 Å, which is the average Au-O bond length within a AuO_4 unit in gold oxide Au_2O_3 .⁶⁰ Furthermore, the values of 93.9° and 86.7° for the two bond angles of O-Au-O around a center gold atom are very similar to those we obtained for the four O-Au-O angles of the AuO_4 units in bulk gold oxide (Au_2O_3) of 91.2°, 94.4°, 86.7°, and 87.6°.⁶⁰ These four angles can be classified into two types, with average values of 92.8° and 87.2°. Thus, there is a strong similarity between the local geometry of the $(2 \times 1)\text{-2O}$ surface oxide with structural building blocks of the bulk gold oxide Au_2O_3 .

The calculated difference electron density distribution of the $(2 \times 1)\text{-2O}$ surface structure is shown in Fig. 8. A depletion of Au $5d$ states of the surface gold atoms bonded to the oxygen atoms is evident, while there is an increase in electron density, and a polarization, on the O atoms. It is interesting to note that these electron redistributions are very similar to those about the O atom, which is twofold coordinated to Au atoms in the low energy surface-oxide-like structure we considered on Au(111) [see Fig. 12(a) of Ref. 8]. In Fig. 9, we show the corresponding PDOS. It can be seen that there is a hybridization between O $2p$ and Au $5d$ orbitals. The valence PDOS for the O atom shows three main regions: bonding states at the bottom of the valence band, a feature at around -1.5 eV, and a large unoccupied peak. The PDOS is rather similar to that of the bulk gold oxide Au_2O_3 described in Ref. 60, which has a notably broader Au $5d$ band as com-

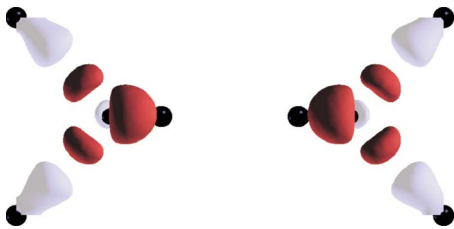


FIG. 8. (Color online) Difference electron densities for the $(2 \times 1)\text{-2O}/\text{Au}(110)$ missing-row structure. The dark (red) isosurfaces indicate an increase in electron density and the light (pale blue) isosurfaces represent a depletion. The black spheres represent the position of the oxygen and gold atoms. The value of the isospheres is $\pm 4.0 \times 10^{-5} e/\text{\AA}^3$.

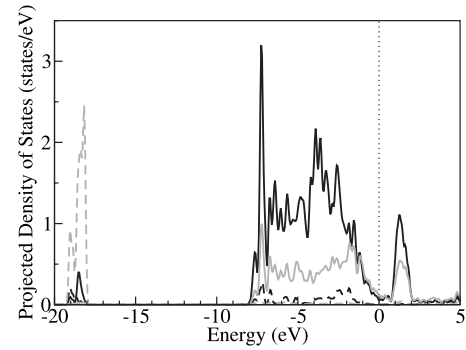


FIG. 9. PDOS for the missing-row $(2 \times 1)\text{-2O}/\text{Au}(110)$ structure. The Au PDOS of the first metal layer atoms that are bonded to oxygen are indicated by dashed ($6s$) and solid ($5d$) dark lines, respectively. The PDOS of O $2s$ and $2p$ states are represented by the dashed and solid gray lines, respectively. The Fermi energy is denoted by the vertical line.

pared to Au_2O_3 , which is hybridized with O $2p$ states, and a high DOS that is unoccupied and characterized by a hybridization of Au $5d\text{-O } 2p$ states. This is consistent with UPS results, which find that the electronic structure of chemisorbed oxygen on Au(110) resembles that of gold oxide Au_2O_3 at 28 K.⁴¹ This suggests that the “chemisorbed oxygen species” bears a close resemblance to this $(2 \times 1)\text{-2O}$ structure. The PDOS for the $(2 \times 1)\text{-2O}$ structure shows a metallic character, while Au_2O_3 is semiconducting. Furthermore, the work function change of this chemisorbed species was reported to be 0.9 eV. We calculated the work function change for the $(2 \times 1)\text{-2O}/\text{Au}(110)$ structure and found a value of 0.82 eV, which is in close agreement with the experimental value.

VI. THERMODYNAMICAL ANALYSIS

In Fig. 10, we show the surface free energy of adsorption [cf. Eq. (3)] for the most favorable structures we investigated for O on the Au(100), Au(110), and Au(111) surfaces. The steeper the gradient, the higher the O coverage. By using Eq. (4), we correlate the oxygen chemical potential with temperature for two selected pressures, namely, that which corresponds to UHV and the other at atmospheric pressure as is characteristic of real pressures employed in technical catalysis. It can be seen that the Au(111) surface-oxide structure is predicted to be stable in a temperature region of 200–420 K for a pressure of 1 atm. For the (110) surface, the missing-row $(2 \times 1)\text{-2O}$ structure is stable at 1 atm to temperatures of around 480 K, while for the Au(100) surface, the added-row $(5 \times 2)\text{-O}$ structure is predicted to be stable up to a temperature of ~ 600 K at atmospheric pressure.

In Fig. 11, to compare the relative surface energies of these structures on a common scale, we plot the surface free energy [cf. Eq. (5)] for the most stable structures of O on the low-index surfaces as a function of oxygen chemical potential, $\Delta\mu_{\text{O}}$. For selected values of $\Delta\mu_{\text{O}}$, we show the predicted nanomorphology of the crystallites by using the Wulff construction. For low values of $\Delta\mu_{\text{O}}$ (< -0.5 eV) the crystal

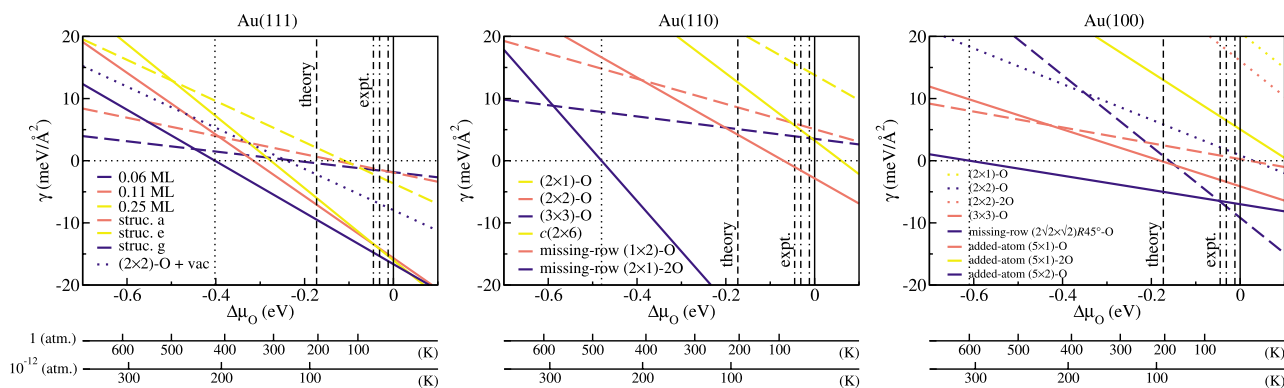


FIG. 10. (Color online) Surface free energies of adsorption [cf. Eq. (3)] for O at Au(111) (left panel), Au(110) (middle panel), and Au(100) (right panel) for the various low energy structures as a function of the O chemical potential, where $\Delta\mu_{\text{O}}$ is defined as $\mu_{\text{O}} - 1/2E_{\text{O}_2}^{\text{total}}$. The corresponding temperatures are given for two selected pressures [cf. Eq. (4)], one corresponding to UHV conditions and the other to atmospheric pressure. For the definition of the oxygen structures on Au(111), we refer to Ref. 8. The dashed vertical line labeled “theory” and the dot-dashed vertical lines labeled “expt.” represent the calculated (Ref. 60) and experimental (Refs. 61–63) values of the heat of formation of bulk Au_2O_3 per O atom. The solid vertical line indicates the energy zero of the change in the O chemical potential with respect to the energy of a free isolated O_2 molecule at absolute zero: $\Delta\mu_{\text{O}} = \mu_{\text{O}} - 1/2E_{\text{O}_2}^{\text{total}}$.

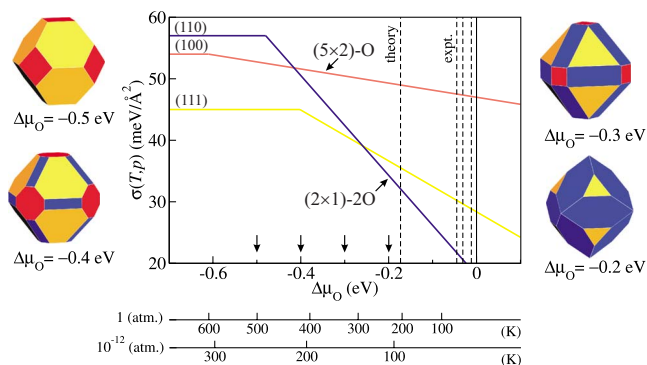


FIG. 11. (Color online) Surface free energies for O at Au(100), Au(110), and Au(111) for the lowest energy structures as a function of the O chemical potential, where $\Delta\mu_{\text{O}}$ is defined as $\mu_{\text{O}} - 1/2E_{\text{O}_2}^{\text{total}}$. For Au(111), Au(110), and Au(100), the most stable structures correspond to the surface-oxide structure reported in Ref. 8 [Fig. 11(g)], the missing-row $(2 \times 1)\text{-}2\text{O}/\text{Au}(110)$ [Fig. 6(e)], and the added-atom $(5 \times 2)\text{-O}/\text{Au}(100)$ [Fig. 2(h)] structures, respectively. The horizontal sections of the dark (blue), gray (red), and light gray (yellow) lines represent the clean surfaces of Au(110), Au(100), and Au(111), respectively. The corresponding temperatures are given for two selected pressures [cf. Eq. (4)], one corresponding to UHV conditions and the other to atmospheric pressure. The predicted nanoparticle shapes are shown for selected values of the oxygen chemical potential as listed (and as indicated by the downward pointing arrows in the plot). For the crystallites, the facets are indicated as follows: midgray (red) (100), dark gray (blue) (110), and light gray (orange) (111). The dashed vertical line labeled “theory” and the dot-dashed vertical lines labeled “expt.” represent the calculated (Ref. 60) and experimental (Refs. 61–63) values of the heat of formation of bulk Au_2O_3 per O atom. The solid vertical line indicates the energy zero of the change in the O chemical potential with respect to the energy of a free isolated O_2 molecule at absolute zero: $\Delta\mu_{\text{O}} = \mu_{\text{O}} - 1/2E_{\text{O}_2}^{\text{total}}$.

shape is dominated by clean Au(111) facets, which have the lowest Gibbs surface free energy for this chemical potential region as well as smaller (100) facets, with the added-row $(5 \times 2)\text{-O}$ structure. As $\Delta\mu_{\text{O}}$ is increased to the range where the surface-oxide-like structures form on the (111) and (110), e.g., at $\Delta\mu_{\text{O}} = -0.4$ eV, the crystal shape now consists of facets of each of these oxygen structures, in addition to the mentioned (100) orientation, where the dominant facet is still (111). As the chemical potential is increased further to, e.g., $\Delta\mu_{\text{O}} = -0.3$ eV, regions of (111) and (100) facets decrease and that of (110) increases. At $\Delta\mu_{\text{O}} = -0.2$ eV, the polyhedron is dominated by (110) facets, covered by the missing-row $(2 \times 1)\text{-}2\text{O}$ structure, and the (100) regions have disappeared. The finding that thin surface-oxide structures on the Au(111) and Au(110) surfaces are predicted to be stable under conditions at which low temperature gold-based catalysts are active indicates that such structures could possibly be present and play a role in the catalytic activity of gold nanoparticles.

Interestingly, the predicted qualitative behavior of the nanogold particles agrees well with recent high-resolution electron microscopy experiments, which include an “environmental sample holder,” where the particles were exposed to a controlled oxygen (or hydrogen) atmosphere and their morphology monitored.⁶⁴ In particular, after cleaning the nanoparticles, which were deposited on both TiO_2 and amorphous carbon, they exhibited (111) and (100) planes, just as we obtained (see Fig. 11 for $\Delta\mu_{\text{O}} = -0.5$ eV). For exposure to oxygen at a pressure of 2 mbars ($\sim 2 \times 10^{-3}$ atm) at room temperature, the particles changed to a “more spherical” shape. These experimental conditions would correspond approximately to $\Delta\mu_{\text{O}} = -0.3$ eV, where the (111) and (100) facets begin to reduce in favor of the presence of (110) planes, which gives a more rounded nature (see Fig. 11 for $\Delta\mu_{\text{O}} = -0.3$ eV). At this value of the oxygen chemical potential, the gold planes are covered with the predicted thin oxy-

gen structures. Experimentally, because this behavior of gold clusters was observed on both TiO_2 and amorphous carbon, it indicates that the shape changes are driven by adsorption on the metal surfaces, as is consistent with our results. Furthermore, the experimental studies investigated the reactivity of the particles for CO oxidation at room temperature, and found, indeed, that a reaction to CO_2 does occur.⁶⁵

VII. CONCLUSIONS

We have studied the O/Au(100) and O/Au(110) systems by using density-functional theory for a range of atomic configurations and oxygen coverages. For O adsorption on Au(100), the most stable structure is the added-atom (5×2)-O configuration, where O adsorbs in a quasi-three-fold hollow site. For adsorption on Au(110), the most stable geometry corresponds to a missing-row (2×1)-2O structure, which may be described as a surface oxide. By using the Gibbs surface free energy, and by including the results of our previous investigation into O adsorption on Au(111), we obtain the predicted Au nanoparticle morphology in an oxidizing environment, using the Wulff construction. At low oxygen chemical potential, clean Au(111) facets dominate. For higher values, e.g., from -0.4 to -0.18 eV, the O-Au surface structures form on all the low-index facets, with the (111) orientation dominating. At atmosphere pressure, this corresponds to a temperature range of 420–200 K. For values of the oxygen chemical potential in the range from -0.26 to -0.18 eV, there is a switchover in that the (110) facets are the dominant region. For a pressure of 1 atm, this corresponds to a temperature range of ~ 300 –200 K. Our results suggest, assuming that O_2 can dissociatively adsorb or atomic oxygen can be supplied from a catalyst support material, that the surface-oxide like structures on the (111), and (2×1)-2O structures on the (110) facets, may be present under low temperature oxidation reaction conditions and could possibly play a role as a catalyst over gold nanoparticles.

ACKNOWLEDGMENTS

We gratefully acknowledge computing resources provided by the Australian Partnership for Advanced Computing

(APAC) National Facility and the Australian Center for Advanced Computing and Communications (ac3). This work was supported by the Australian Research Council (ARC). We thank A. Soon for helpful discussions.

APPENDIX: CONVERGENCE TESTS FOR SURFACE ENERGIES

Convergence tests have been carried out for the surface energies of Au(100) and Au(110) with regard to the \mathbf{k} -point sampling, energy cutoff, and number of atomic layers in the symmetric slab. For the Au(110) surface, we used a (2×1) SUC and calculated the unreconstructed and missing-row surface energies. We tested \mathbf{k} -point sets of $4 \times 12 \times 1$ (21 \mathbf{k} points in the IBZ) and $5 \times 15 \times 1$ (24 \mathbf{k} points in the IBZ), where the total energy differed by only 0.0044 eV for the unreconstructed surface and 0.027 eV for the missing-row surface per SUC. Furthermore, we tested energy cutoffs of 500 and 600 eV, where the total energy differed by only 0.0006 eV for the unreconstructed surface and 0.0007 eV for the missing-row surface per SUC. We also tested the number of atomic layers in the slab. For the unreconstructed surface, we found that the surface energy per SUC is 1.38 eV for the case of 7, 9, and 11 layers. For the missing-row surface, the surface energies per SUC are 1.36 (7 layers), 1.29 (9 layers), and 1.28 eV (11 layers). Thus, we regard the surface energy to be converged at seven layers for the unreconstructed clean surface, and at nine layers for the missing-row surface.

For the Au(100) surface, we used both a (1×1) and (5×1) SUC to calculate the clean unreconstructed surface energy. We tested \mathbf{k} -point sets of $3 \times 15 \times 1$ (16 \mathbf{k} points in the IBZ) and $4 \times 20 \times 1$ (33 \mathbf{k} points in the IBZ), and found that the surface energy per SUC is practically identical. Furthermore, we tested energy cutoffs of 500 and 600 eV, where the total energy differed by only 0.0015 eV per SUC. We also tested the number of atomic layers in the slab. We found that the surface energy per SUC differed only by 0.01 eV between a six-layer and an eight-layer slab. Furthermore, we used a (1×1) SUC to calculate the clean unreconstructed surface energy and found that the surface energy is identical to that obtained from the (5×1) SUC. Thus, our results, as presented for the described calculation parameters, are highly converged.

¹G. C. Bond and D. T. Thompson, *Catal. Rev. - Sci. Eng.* **41**, 319 (1999).

²M. Haruta, N. Amada, T. Kobayashi, and S. Iijima, *J. Catal.* **115**, 301 (1989).

³M. Haruta, *Gold Bull.* **37**, 27 (2004), and references therein.

⁴R. Meyer, C. Lemire, Sh. K. Shaikhutdinov, and H.-J. Freund, *Gold Bull.* **37**, 72 (2004), and references therein.

⁵C. T. Campbell, *Science* **306**, 234 (2004).

⁶B. K. Hodnett, *Heterogeneous Catalytic Oxidation* (Wiley, Chichester, UK, 2000).

⁷J. K. Nørskov, T. Bligaard, A. Logadottir, S. Bahn, L. B. Hansen, M. Bollinger, H. Bengaard, B. Hammer, Z. Sljivancanin, M.

Mavrikakis, Y. Xu, S. Dahl, and C. J. H. Jacobsen, *J. Catal.* **209**, 275 (2002).

⁸H. Q. Shi and C. Stampfl, *Phys. Rev. B* **76**, 075327 (2007).

⁹Ch. Wöll, S. Chiang, R. J. Wilson, and P. H. Lippel, *Phys. Rev. B* **39**, 7988 (1989).

¹⁰M. A. Chesters and G. A. Somorjai, *Surf. Sci.* **52**, 21 (1975).

¹¹M. E. Schrader, *Surf. Sci.* **78**, L227 (1978).

¹²N. D. S. Canning, D. Outka, and R. J. Madix, *Surf. Sci.* **141**, 240 (1984).

¹³P. Legaré, L. Hilaire, M. Sotto, and G. Maire, *Surf. Sci.* **91**, 175 (1980).

¹⁴J. J. Pireaux, M. Chtaïb, J. P. Delrue, P. A. Thiry, M. Liehr, and R.

- Caudano, Surf. Sci. **141**, 211 (1984).
- ¹⁵J. J. Pireaux, M. Liehr, P. A. Thiry, J. P. Delrue, and R. Caudano, Surf. Sci. **141**, 221 (1984).
- ¹⁶D. H. Parker and B. E. Koel, J. Vac. Sci. Technol. A **8**, 2585 (1990); M. A. Lazaga, D. T. Wickham, D. H. Parker, G. N. Kastanas, and B. E. Koel, ACS Symp. Ser. **523**, 90 (1993).
- ¹⁷A. Krozer and M. Rodah, J. Vac. Sci. Technol. A **15**, 1704 (1997).
- ¹⁸D. E. King, J. Vac. Sci. Technol. A **13**, 1247 (1995).
- ¹⁹F. Cotton and G. Wilkinson, *Inorganic Chemistry*, 3rd ed. (Wiley, New York, 1972), p. 994.
- ²⁰N. Saliba, D. H. Parker, and B. E. Koel, Surf. Sci. **410**, 270 (1998).
- ²¹K. A. Davis and D. W. Goodman, J. Phys. Chem. B **104**, 8557 (2000).
- ²²J. Cao, N. Wu, S. Qi, K. Feng, and M. S. Zei, Chin. Phys. Lett. **6**, 92 (1989).
- ²³J. Chevrier, L. Huang, P. Zeppenfeld, and G. Comsa, Surf. Sci. **355**, 1 (1996).
- ²⁴L. Huang, J. Chevrier, P. Zeppenfeld, and G. Comsa, Appl. Phys. Lett. **66**, 935 (1995).
- ²⁵L. Huang, J. Chevrier, P. Zeppenfeld, and G. Comsa, Appl. Phys. Lett. **66**, 935 (1995); L. Huang, P. Zeppenfeld, J. Chevrier, and G. Comsa, Surf. Sci. **352**, 285 (1996); J. Chevrier, L. Huang, P. Zeppenfeld, and G. Comsa, *ibid.* **355**, 1 (1996); Y. Uchida, X. Bao, K. Weiss, and R. Schlögl, *ibid.* **401**, 469 (1998); L. Ortega, L. Huang, J. Chevrier, P. Zeppenfeld, J. M. Gay, F. Rieutord, and G. Comsa, Surf. Rev. Lett. **4**, 1315 (1997).
- ²⁶Y. Uchida, X. Bao, K. Weiss, and R. Schlögl, Surf. Sci. **401**, 469 (1998).
- ²⁷X. Bao, J. V. Barth, G. Lehmppfuhl, R. Schuster, Y. Uchida, R. Schlögl, and G. Ertl, Surf. Sci. **284**, 14 (1993).
- ²⁸H. Schubert, U. Tegtmeyer, D. Herein, X. Bao, M. Muhler, and R. Schlögl, Catal. Lett. **33**, 305 (1995).
- ²⁹S. M. McClure, T. S. Kim, J. D. Stiehl, P. L. Tanaka, and C. B. Mullins, J. Phys. Chem. B **108**, 17952 (2004).
- ³⁰X. Y. Deng, B. K. Min, A. Guloy, and C. M. Friend, J. Am. Chem. Soc. **127**, 9267 (2005).
- ³¹B. K. Min, X. Deng, D. Pinnaduwwage, R. Shalek, and C. M. Friend, Phys. Rev. B **72**, 121410(R) (2005).
- ³²Z. P. Liu, P. Hu, and A. Alavi, J. Am. Chem. Soc. **124**, 14770 (2002).
- ³³M. A. Van Hove, R. J. Koestner, P. C. Stair, J. P. Biberian, L. Kesmodel, I. Bartos, and G. A. Somorjai, Surf. Sci. **103**, 189 (1981); **103**, 218 (1981).
- ³⁴K. H. Rieder, T. Engel, R. H. Swendsen, and M. Manninen, Surf. Sci. **127**, 223 (1983).
- ³⁵G. K. Binnig, H. Rohrer, Ch. Gerber, and E. Stoll, Surf. Sci. **144**, 321 (1984).
- ³⁶B. W. Dodson, Phys. Rev. B **35**, 880 (1987).
- ³⁷V. Fiorentini, M. Methfessel, and M. Scheffler, Phys. Rev. Lett. **71**, 1051 (1993).
- ³⁸I. K. Robinson, Phys. Rev. Lett. **50**, 1145 (1983); I. K. Robinson, Y. Kuk, and L. C. Feldman, Phys. Rev. B **29**, 4762 (1984).
- ³⁹L. D. Marks, Phys. Rev. Lett. **51**, 1000 (1983).
- ⁴⁰W. Moritz and D. Wolf, Surf. Sci. **163**, L655 (1985).
- ⁴¹J. M. Gottfried, K. J. Schmidt, S. L. M. Schroeder, and K. Christmann, Surf. Sci. **525**, 197 (2003).
- ⁴²G. Kresse and J. Hafner, Phys. Rev. B **47**, 558 (1993); **49**, 14251 (1994).
- ⁴³G. Kresse and J. Furthmüller, Comput. Mater. Sci. **6**, 15 (1996).
- ⁴⁴G. Kresse and J. Furthmüller, Phys. Rev. B **54**, 11169 (1996).
- ⁴⁵G. Kresse and D. Joubert, Phys. Rev. B **59**, 1758 (1999).
- ⁴⁶P. E. Blöchl, Phys. Rev. B **50**, 17953 (1994).
- ⁴⁷J. P. Perdew, J. A. Chevary, S. H. Vosko, K. A. Jackson, M. R. Pederson, D. J. Singh, and C. Fiolhais, Phys. Rev. B **46**, 6671 (1992).
- ⁴⁸J. Neugebauer and M. Scheffler, Phys. Rev. B **46**, 16067 (1992).
- ⁴⁹M. Scheffler and C. Stampfl, in *Electronic Structure*, edited by K. Horn and M. Scheffler, Handbook of Surface Science Vol. 2 (Elsevier, Amsterdam, 1999).
- ⁵⁰W. X. Li, C. Stampfl, and M. Scheffler, Phys. Rev. B **65**, 075407 (2002).
- ⁵¹K. Reuter and M. Scheffler, Phys. Rev. B **65**, 035406 (2001).
- ⁵²C. Kittel, *Introduction to Solid State Physics* (Wiley, New York, 1996).
- ⁵³B. D. Yu and M. Scheffler, Phys. Rev. B **56**, R15569 (1997).
- ⁵⁴L. L. Wang and H. P. Cheng, Phys. Rev. B **69**, 165417 (2004).
- ⁵⁵A. Kokalj, A. D. Corso, S. Gironcoli, and S. Baroni, J. Phys. Chem. B **110**, 367 (2006).
- ⁵⁶M. Gajdoš, A. Eichler, and J. Hafner, Surf. Sci. **531**, 272 (2003).
- ⁵⁷K. Berge and A. Goldmann, Surf. Sci. **540**, 343 (2003).
- ⁵⁸W. X. Li, L. Österlund, E. K. Vestergaard, R. T. Vang, J. Matthiesen, T. M. Pedersen, E. Lægsgaard, B. Hammer, and F. Besenbacher, Phys. Rev. Lett. **93**, 146104 (2004).
- ⁵⁹R. Feidenhans'l, F. Grey, M. Nielsen, F. Besenbacher, F. Jensen, E. Laegsgaard, I. Stensgaard, K. W. Jacobsen, J. K. Nørskov, and R. L. Johnson, Phys. Rev. Lett. **65**, 2027 (1990).
- ⁶⁰H. Q. Shi, R. Asahi, and C. Stampfl, Phys. Rev. B **75**, 205125 (2007).
- ⁶¹*The Oxide Handbook*, edited by G. V. Samsonov (IFI/Plenum, New York, 1982).
- ⁶²*Handbook of Chemistry and Physics*, edited by R. C. Weast, M. J. Astle, and W. H. Beyer (Chemical Rubber Company, Boca Raton, FL, 1989), Vol. 69.
- ⁶³O. Kubaschewski, C. B. Alcock, and P. J. Spencer, *Materials Thermochemistry* (Pergamon, Oxford, 1993).
- ⁶⁴S. Giorgio, S. Sao Joao, S. Nitsche, D. Chaudanson, G. Sitja, and C. R. Henry, Ultramicroscopy **106**, 503 (2006).
- ⁶⁵P. L. Gai, E. D. Boyes, S. Helveg, P. L. Hansen, S. Giorgio, and C. R. Henry, MRS Bull. **32**, 1044 (2007).